Biomass Conversion and Biorefinery (2023) 13:15267–15279
https://doi.org/10.1007/s13399-022-03567-x

ORIGINAL ARTICLE

Application of the SCE optimization algorithm in determining thermal decomposition kinetics of *Pinus radiata* needles and *Eucalyptus globulus* leaves

Andrés Arriagada[1] · Jorge Contreras[2] · Jean-Louis Consalvi[3]

Received: 11 August 2022 / Revised: 3 November 2022 / Accepted: 15 November 2022 / Published online: 29 November 2022

Abstract
The goal of this work was to study the thermal decomposition kinetics of two exotic Chilean wildland fuels, namely, *Pinus Radiata* (PR) needles and *Eucalyptus Globulus* (EG) leaves, by using thermogravimetric analysis (TGA) experiments, and the shuffled complex evolution (SCE) technique to estimate kinetic parameters through an inverse optimization process, and 0D simulations to validate a kinetic model against experimental mass loss rates (MLR). TGA experiments were monitored under inert (N_2) and oxidative (air) atmospheres at a temperature range from 200 to 600 °C. Analyses were performed at four heating rates of 5, 10, 15, and 20 °C min^{-1}. We demonstrated the effectiveness of the SCE algorithm in determining solid-phase kinetics parameters by correlating several reaction mechanisms of inert and oxidative decomposition with experimental TGA data. Optimized parameters were used in the Gpyro simulation suite to predict MLR. Results show that, under inert conditions, the conversion from dry fuel to char can be modeled with a three-step mechanism for both species. Under oxidative conditions, the analysis showed that MLR could be predicted with a good fit using a five-step reaction kinetic mechanism for EG leaves, and four reactions for PR needles. Finally, a set of kinetic parameters is proposed for thermal decomposition models.

Keywords Wildland fuels · Pyrolysis · Multi-step reaction mechanisms · Thermal decomposition · Thermogravimetric analysis · Optimization

1 Introduction

Pinus radiata (PR) and *Eucalyptus globulus* (EG) are the most important forest resources in Chile, with approximately 2.87 million hectares of these non-indigenous species, equivalent to 17.2% of its total forests. Of this area, 68% is PR; followed by EG, 23% [1]. This has an enormous energy potential but is also an important menace when it is not properly managed due to the increasing forest fires over time [2]. Wildland fires in Chile have increased in frequency and surface burnt in the past four decades, risking human lives and property every fire season—especially as more people claim wildland areas [3]. These forest species are flammable and extremely flammable, which means, they have a high susceptibility to ignite [4, 5]. Furthermore, forestry industry plays a crucial role in the Chilean economy, being the first sector in renewable resources [6]. In this scenario, biomass has been also identified as an auspicious option for H_2 and syngas production, due to its abroad availability, sustainable life cycle for CO_2, and transportation flexibility [7, 8].

One of the primary energy sources for wildfires is wildland fuel litter, the bottom level of the forest, composed of dead needles and leaves. Given the percentage of PR and EG in Chile, their leaf litter is, under dry conditions, a significant contributor to wildland fires. If a fire starts in this zone, the thermal decomposition behavior of these litters will determine the fire spread [9]. Indeed, sustainable combustion of these detritus is determined by the available quantity of gaseous fuel in the flaming zone, which is controlled

✉ Andrés Arriagada
andres.arriagada@usm.cl

[1] Department of Mechanical Engineering, Universidad Técnica Federico Santa María, Av. España 1680, Valparaíso, Chile

[2] EPROIC Ingeniería Y Construcción Ltda, Viña del Mar, Chile

[3] Aix-Marseille Université, IUSTI/UMR CNRS 7343, 5 Rue E. Fermi, 13453 Marseille Cedex 13, France

by the rate of mass loss (ML) of the solid wildland fuel because of being exposed to high radiative heat fluxes. In this regard, understanding the thermal decomposition process of wildland fuels is decisive for further wildland fire safety development [10], and for studying the potential of these fuels as alternative energy [11–13].

Traditional kinetic models for wildland fuels—predictions of solid fuel thermal decomposition and gaseous pyrolysis products processes—involve numerous parameters that are time-consuming and difficult to measure and made more difficult still due to the complexity of fuel composition and its influence on fire ignition and spread [14]. Most physically based models used a simplified three-step reaction mechanism [15–19]: first, drying of wet wildland fuel (WWF) as it converts to dry wildland fuel (DWF) and water vapor; second, pyrolysis of DWF as it converts to char and gaseous products; and third, char oxidation [20]. In such thermal decomposition models, kinetics parameters are estimated from experimental data.

Here, experimental data for thermal decomposition studies usually come from TGA, a tool for preliminary kinetics studies in the thermal decomposition of solids [21–23] and that can identify individual components and/or intermediate species throughout the entire thermal decomposition process to improve the understanding of mass loss kinetics [24, 25]. This method has been used to characterize the thermal decomposition of Mediterranean plant species under oxidative conditions and to assess their potential combustibility as natural fuels [26, 27]. Furthermore, Gerandi et al. [28] used TGA to validate three kinetic mechanisms to predict the thermal decomposition of untreated wood plates of oak and eucalyptus at matter and material scales. Next, in a study modeling biomass pyrolysis kinetics of vegetative species using a sequential multi-step reaction model, Burra and Gupta [29] used TGA results as input for kinetics parameters. Other studies have subjected live and dead wildland vegetation from 14 species to TGA at five heating rates (from 10 to 30 °C min^{-1}) [30], obtaining pyrolysis kinetics using the Kissinger–Akahira–Sunose (KAS) method as a function of conversion. From an energy source perspective, Cumming and McLaughlin [31] used oxidative TGA profiles for an initial evaluation of industrial-scale combustion behavior toward the design and operation of conversion systems [32]. The effect of retardants on pine needles' thermal decomposition was studied by [33] using differential thermal analysis (DTG) under a nitrogen atmosphere. These researchers compared DTG curves of *Pinus halepensis* needles with different quantities of retardant and analyzed curve differences, but the authors did not obtain kinetics parameters. Wadhwani et al. [34] studied the kinetics of pyrolysis of litter materials from pine and eucalyptus forests by using TGA experiments under nitrogen, reviewing several models to find the most pertinent of the samples studied; the authors found that the most suitable reaction model was identified as the Johnson–Mehl–Avrami model.

Regarding modeling, genuinely detailed descriptions of phenomena in physically based models require many computational resources—further increased when replacing the widely used one-step mechanism with any more complex thermal decomposition description of wildland fuel. As a matter of fact, Benkorichi et al. [20] assessed increasing levels of complexity in predicting the thermal decomposition of *Pinus pinaster* needles under inert and oxidative TGA at four heating rates, concluding that, after drying, three-step and six-step mechanisms were the minimum to predict pyrolysis, under inert and oxidative conditions, respectively. The accuracy and uncertainty of multi-step kinetic mechanisms were further explored by Richter and Rein [35] who studied 1 to 12 reaction mechanisms across seven species, finding that increasing parameters increased uncertainty but not necessarily accuracy. Thus, several numerical tools have been developed to simulate solid pyrolysis, mass loss, and heat transport—such as Fire Dynamics Simulator (FDS) pyrolysis sub-model [36], Gpyro [37], Thermakin [38], Pyropolis [7], or the FireFOAM pyrolysis model [39–41]—there is still need to make use of microscale experiments as an initial step to test and predict more complex models.

Thus, using the most populous non-native wildland species in Chile, this study aims to propose a kinetic framework to study the thermochemical conversion of PR needles and EG leaves from solid to gaseous fuel assessing the capability of multi-step kinetics mechanisms under different atmospheres to predict MLR.

2 Methods

A set of kinetic parameters were obtained from both empirical TGA and numerical pyrolysis model predictions, with a near-optimal agreement. In this latter, parameters obtained were input to the Gpyro pyrolysis model [42] to run simulations of MLR, focusing on thermal decomposition kinetics and MLR to represent the velocity at which gaseous fuel products are being produced. Sample preparation, characterization, estimation, simulation, and comparisons are discussed below.

2.1 Sample preparation

Wildland fuel litter (EG leaves and PR needles) were collected near Valparaíso, Chile (33°03'S, 71°37'W). After field sampling, fuel elements were oven-dried at 60 °C for 24 h. Such drying is a single-step reaction with well-established kinetics parameters [20]. Although no further changes in mass due to moisture were observed, sample loading of

leaves and needles before each test indicated weak moisture content (1–3%), likely due to self-rehydration.

2.2 Physicochemical characterization and TGA

Elemental analysis of EG leaves and PR needles revealed carbon (C), hydrogen (H), nitrogen (N), and sulfur (S) element weight contents (Thermo Finnigan Flash EA), with the weight percent of oxygen (O) determined by difference. Proximate analysis was performed according to ASTM standards E 1102–84, E 872–82, and E 870–82 for ash, volatile matter (VM), and fixed carbon (FC), respectively [43]. Next, experimental thermogravimetric data was generated (TA-Instrument TGA Q50) under non-oxidative (nitrogen) and oxidative (air) conditions to evaluate kinetics in purely pyrolytic and oxidative conditions. Pulverized samples (22 µL) were conditioned in an open platinum crucible (5000 ± 0.01 mg) at atmospheric pressure (flow rate of 40 mL min^{-1}) at four different heating rates (5, 10, 15, 20 °C min^{-1}).

2.3 Optimization algorithm and simulation methodology

Kinetic parameters were estimated using an automated optimization procedure based on evolutionary algorithms, following Lautenberger and Fernandez-Pello [44]. The shuffled complex evolution (SCE) optimization algorithm [45–47] is an evolutionary algorithm that performs a local and global search to estimate kinetics parameters, combining the competitive complex evolution and the simplex method. According to Duan et al. [46], the SCE technique converges to a global optimum, being robust, effective, and efficient for several applications. This technique was selected for this research purposes, following the literature [20, 46–49], which evaluated optimization tools using Gpyro; furthermore, of several optimization methods recently evaluated for microscale biomass pyrolysis modeling, SCE was confirmed as performing better [50]. This inverse problem is ill-posed—that is, the solution (the set of kinetic parameters) is not necessarily unique nor necessarily stable to small changes in the input data—this optimization process is meant to be heuristic, not necessarily the absolute optimal solution. Regardless, the algorithm presented a near-optimal prediction of the experimental data given the constraints of the underlying physical model.

Furthermore, such genetic and evolutionary algorithms have been widely used in engineering, e.g., SCE applied combustion and chemical kinetics optimization problems, including heterogeneous [44, 51, 52] and homogeneous [52, 53] reaction mechanisms. Additionally, while solution uniqueness (i.e., the kinetics parameter set) is always a concern in inverse problems, it may be abated by using four different heating rates as in the present work (5, 10, 15, and 20 °C min^{-1}). In short, although inverse optimization techniques are not free of criticism [55], they remain one of the best options for performing the task [50].

In simulating thermal decomposition kinetics, this study used Gpyro version 0.8186, an open-source, generalized pyrolysis model developed by Lautenberger et al. [37, 42, 44]. Gpyro can model a zero-dimensional transient mode, intended to represent lumped systems with negligible temperature and species gradients, as occurs in ideal TGA experiments. Kinetics mechanisms of increasing complexity were assessed under oxidative and inert atmospheres [20]. The results show that, for inert and oxidative atmospheres, three-step and six-step mechanisms perform best, respectively. These intermediate reactions were used for simulations during this study. The kinetic scheme adopted in the present study includes the following reactions:

$$DWF \rightarrow \nu_1(a - Specie) + \left(1 - \nu_1\right)Gas \tag{1}$$

$$(a - Specie) \rightarrow \nu_2(\beta - Specie) + (1 - \nu_2)Gas \tag{2}$$

$$(\beta - Specie) \rightarrow \nu_3 Char + (1 - \nu_3)Gas \tag{3}$$

$$(a - Specie) \rightarrow \nu_4(\beta - Specie) + (1 - \nu_4)Gas \tag{4}$$

$$(\beta - Specie) \rightarrow \nu_5 Char + (1 - \nu_5)Gas \tag{5}$$

$$Char \rightarrow \nu_6 Ash + (1 - \nu_6)Gas \tag{6}$$

In the previous scheme, we have reactions 1 to 3 (R1 to R3) that are used to simulate thermal degradation under inert atmospheres. The first step reaction (R1) is related to the conversion of the Dry-Specie into an intermediate specie called α-Specie and gaseous pyrolysis products. Next, another reaction (R2) converts α-Specie to β-Specie. Finally, the β Specie goes into the final reaction to form char (R3). When thermal degradation is assessed under oxidative conditions, reactions R4 and R5 allow accounting for oxidative pyrolysis, and reaction R6 assesses char oxidation.

While the governing equations in 0D can be used to estimate differential thermogravimetric curves (for a detailed explanation, see ref. [56]), we reproduce here the final equations.

$$\frac{d}{dt}\left(\frac{m''}{m_0''}\right) = \frac{\dot{\omega}_{fg}'''\Delta z}{m_0''} = -\frac{\dot{\omega}_{fg}'''\Delta z}{(\overline{\rho}\Delta z)|_{t=0}} \tag{7}$$

where m'' is the mass, m_0'' is the initial mass (in $t = 0$), $\dot{\omega}_{fg}'''$is the reaction rate, $\overline{\rho}$ is the average density, and Δz is the grid size. Integrating the differential thermogravimetric curve yields a thermogravimetric curve:

$$\frac{m''}{m''_0}(t) = 1 - \frac{1}{m''_0}\int_0^t \dot{\omega}'''_{fg}(\tau)\Delta z(\tau)d\tau \quad (8)$$

Moreover, the reaction rate ($\dot{\omega}'''_i$) is given by:

$$\dot{\omega}'''_i = Aexp\left(-\frac{E_a}{RT}\right)m_i^n \quad (9)$$

where A is the pre-exponential factor [s^{-1}]; E_a, activation energy [kJ mol^{-1}]; R, universal gas constant; T, temperature [°C]; n, reaction order; and m_i, mass of reactant i. These parameters were calculated for each species under study for use in the thermal decomposition model to predict MLR. In the case reactions affected by oxygen (O_2), the reaction rate is proportional to $\left(1 + Y_{O_2}\right)^{n_{O_2}}$, where Y_{O_2} is the local value of oxygen mass fraction in the decomposing solid and n_{O_2} is the reaction order that controls the oxygen sensitivity of the process [37].

3 Results and discussion

We describe the kinetic behavior of thermal decomposition, as determined by MLR, i.e., the velocity at which gaseous fuel products are produced. Typically, the first process found in the thermal decomposition process of wildland fuels at ambient temperature is the drying process, from wet wildland fuel (WWF) to dry wildland fuel (DWF). However, since the drying process can be described by a single-step reaction with well-established kinetic parameters [20]—and since the generation of organic decomposition products is known to begin at around 200 °C and to attain maximum reaction rates between 250 and 450 °C [57, 58]—the results studied in the present paper are in the temperature range of 200–600 °C. The fuel density of EG leaves and PR needles was found to be 833 and 719 g/cm^3, respectively, confirming previous studies [59]. Below, we discuss results for inert and oxidative atmospheres: first, we provide an elemental and proximal analysis of the species under study. Second, we analyze experimental TGA results, present optimized kinetic parameters, and then compare the predicted results of MLR for each species to the corresponding experimental results. Finally, we analyze the predicted reaction rates in terms of how thermal decomposition is produced for each wildland species.

3.1 Elemental and proximate analysis

Elemental and proximate analyses were conducted to explore whether TGA results could be influenced by the inherent composition of PR and EG species (Table 1). Proximate analysis shows EG leaves have approximately 50% more ash than, but only a third of the fixed carbon (FC) of, PR needles. The volatile matter (VM) was quite similar for both species, with high energy values. Although such volatile matter increases fire hazards, it could also be considered an alternative suitable for pyrolysis, gasification, or combustion processes [60]. However, ash content may increase fouling in reactors, instigating higher processing costs, poor combustion, disposal problems, and low energy conversion [61]. The possibility of using these wildland fuels as an energy source should be further investigated.

Regarding elemental analysis, both species are carbon-rich and have similar hydrogen (H) content. Sulfur (S) content found is less than 0.4, in line with what has been reported in the literature [66]. However, the nitrogen (N) content of EG is around 50% higher than PR's.

3.2 Experimental results under an inert atmosphere

Figure 1 shows mass evolution in EG leaves (a) and PR needles (b) under nitrogen as a function of temperature for the four different heating rates studied here (5, 10, 15, and 20 °C min^{-1}). The ML curves are similar for both EG and PR species, regardless of heating rate. Between 200 and 300 °C, approximately 22% of the mass of EG leaves is lost (Fig. 1a); at 300–400 °C (where the highest MLR peak is found, see Fig. 2a), about 28% of the initial mass is devolatilized, to 50% at 400 °C; between 400 and 500 °C, around 17% of the initial mass is lost; and from 500 to 600 °C, only 3% of the initial mass is gasified. The residue left at the end of the test was about 30% of the initial mass, regardless of heating rate; however, the proximate analysis indicated that volatile matter is around 80%, so 10% could still be gasified after 600 °C if oxygen were available.

Table 1 Comparison of elemental and proximate analyses with literature data. All data is reported in g/100 g of dried sample

Wildland fuel	Proximate analysis			Elemental analysis				
	VM	FC	Ash	C	H	O	N	Ref
EG	81.2	3.7	15.1	51.1	7.3	30.1	1.56	Measured
	82.62	16.15	1.23	47.1	6.0	45.43	-	[62]
	81.1	18.3	0.60	51.0	5.8	45.30	-	[63]
PR	80.4	10.0	9.60	49.4	7.4	35	0.96	Measured
	72.38	26.12	1.50	48.21	6.57	43.72	-	[64]
	76.50	14.45	0.89	49.41	7.67	42.19	-	[65]

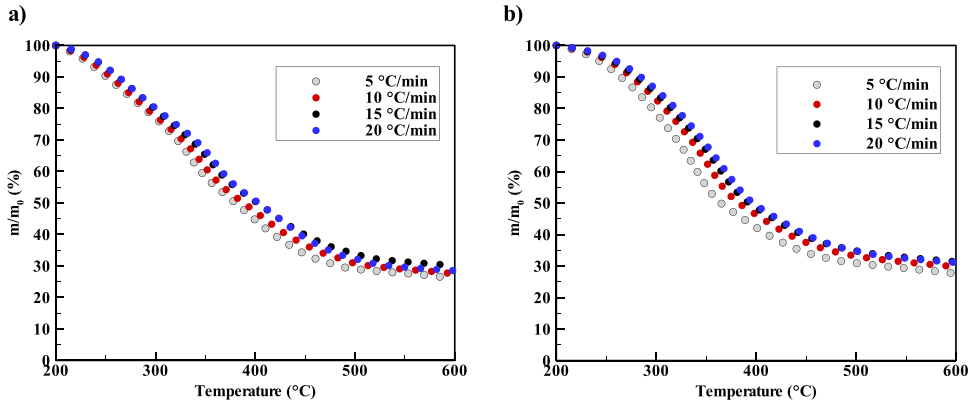

Fig. 1 Evolution of experimental thermogravimetric ML as a function of the temperature under inert atmosphere for **a** EG leaves and **b** PR needles

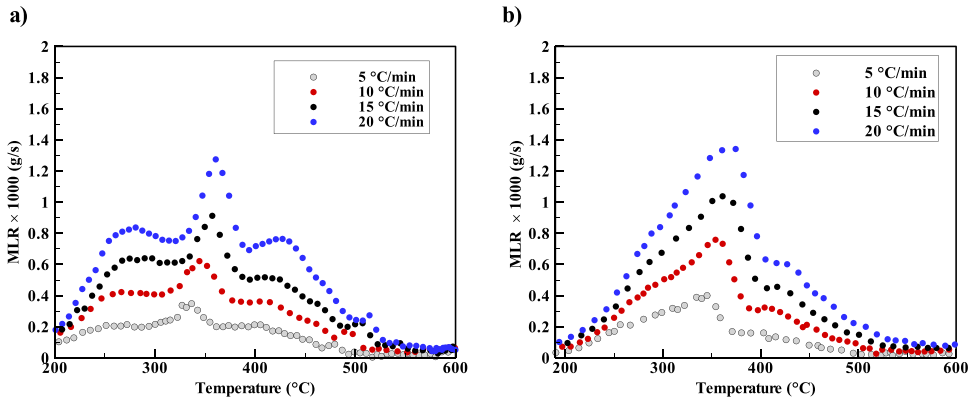

Fig. 2 Evolution of the experimental MLR as a function of the temperature under an inert atmosphere for **a** EG leaves and **b** PR needles

In the case of PR (Fig. 1b), at a heating rate of 20 °C min^{-1}, from 200 and 300 °C, 15% of the initial mass was lost; between 300 and 400 °C, 35%; from 400 to 500 °C, around 15% is devolatilized; and finally, from 500 to 600 °C, 4% of the initial mass is lost. Approximately 31% of the initial mass remains at the end of the test. However, at a heating rate of 5 °C min^{-1}, the mass loss is significantly faster between 300 and 500 °C, although not so for EG leaves. This result is consistent with ref. [66] since higher heating rates may increase char formation, imbuing thermal resistance to heat transfer. For example, between 200 and 300 °C, 22 and 15% of PR mass is lost for heating rates of 5 and 20 °C min^{-1}, respectively; and at 400 °C, about 58 and 50% of the initial PR mass has been devolatilized for heating rates of 5 and 20 °C min^{-1}, respectively. The remaining mass at the end of the 5 °C min^{-1} test is around 27%, versus 31% for 20 °C min^{-1}.

Figure 2 plots the derived MLR for EG leaves (a) and PR needles (b) as a function of temperature, under an inert atmosphere, for the four heating rates. Thermal decomposition of EG leaves (Fig. 2a) started around 200 °C for every heating rate, although the following peak and shoulders are more pronounced at higher heating rates. The first shoulder, around 270 °C, coincides with 12% ML; the peak, at approximately 350 °C, with 60% mass lost, and the second shoulder, around 430 °C, where char formation reaches its maximum. Shoulders and peaks are likely where lignin liberates volatiles and causes significant ML and MLR.

The presence of shoulders is uncommon for TGA under pure pyrolytic conditions. Although the literature reports one peak under pure pyrolytic conditions for Eucalyptus leaves [63, 64] and two for Eucalyptus sawdust [67], no noticeable shoulders have been reported. The results in this paper may, however, be due to the decomposition of the three main biomass components, more closely matching DiBlasi's [68] determined primary and relative contribution to decomposition rates of cellulose, hemicellulose, and lignin. Indeed, heating rates at sufficiently slow or moderate temperatures induce several zones in the mass loss curves associated with component dynamics: hemicelluloses decompose at 225–325 °C; cellulose at 325–375 °C; and lignin, gradually over 250–500 °C [69].

As expected, the heating rate also influenced the effective thermal decomposition temperature range. Increased heating rates resulted in lower thermal decomposition at higher temperatures, most likely due to the material not fully reaching that temperature in a shorter time, a process known as thermal lag [60]. Indeed, the onset of devolatilization consistently shifted to higher values for heating rates of 5, 10, 15, and 20 °C min^{-1}, and MLR peaks occurred around 335, 347,

356, and 360 °C, respectively. The heating rate had a more pronounced effect on absolute peak thermal decomposition rates, which increased to 0.36, 0.61. 0.9, and 1.28 at 5, 10, 15, and 20 °C min^{-1}, respectively.

For PR needles (Fig. 2b), results also show one peak and two shoulders between 200 and 450 °C, although the first shoulder is significantly less pronounced than in EG. Similarly, increased PR heating rates increase MLR and shift peak temperature higher. The first shoulder is between 200 and 250 °C or 345–370 °C, depending on the heating rate; the peak, at around 370 °C; and the second, between 370 and 410 °C. Between 410 and 530 °C, MLR sharply decreases to no devolatilization. Indeed, thermal decomposition rates above 530 °C are significantly reduced as in EG leaves, suggesting a limit for inert pyrolysis.

Estimations under an inert atmosphere.

To estimate kinetics parameters (verifiable) to reproduce MLR numerically, we used the shuffled complex evolution optimization process applied to experimental data, following Lautenberg and colleagues [44]. Optimized parameters for each species are given in Table 2.

To evaluate these optimized parameters, a simulation of the thermal decomposition process was run using the three-step mechanism for inert atmospheres proposed by Benkorichi et al. [20]. This three-step mechanism is detailed in reactions R4 to R6.

Figure 3 compares numerical predictions and experimental results for the evolution of MLR as a function of the temperature for EG leaves (a) and PR needles (b) for the four heating rates. For EG leaves (Fig. 3a), after the first shoulder at 300 °C, the proposed mechanism and optimized kinetics parameters appear to agree with the experimental data for the four heating rates. Peak magnitudes are also well reproduced for 5 and 10 °C min^{-1}. However, at 15 and 20 °C min^{-1}, peak MLR is slightly underpredicted. Simulations also captured heating rate effects on increased and shifted peaks.

The predicted MLR for PR needles (Fig. 3b) also agreed well with experimental data, regardless of the heating rate. The simulation captured thermal decomposition onset at 200 °C, the slight shoulder at around 300 °C, the magnitude and position of the principal peak at around 350 °C, and, while this model failed to capture the second shoulder (around 400 °C), it remained in good agreement with the final MLR decrease.

By way of example, the predicted three-step mechanism reaction rates at a heating rate of 20 °C min^{-1} are shown in Fig. 4a, and b for EG leaves and PR needles, respectively. The EG leaf reaction rates (a) suggest that the initial conversion of DWF to α-eucalyptus is responsible for the first shoulder at around 250 °C; the second and most considerable, converting α-eucalyptus to β-eucalyptus, closely predicts the central peak at 350 °C; and the final, β-eucalyptus

Table 2 Estimated kinetic parameters of different mechanisms under an inert atmosphere for EG and PR

Species	Reagent	Product	Kinetics parameters		
			Log_A (s^{-1})	E_a (kJ mol^{-1})	n (-)
EG	Dry-eucalyptus	α-eucalyptus	6.58	86.98	4.49
	α-eucalyptus	β-eucalyptus	9.01	132.7	0.78
	β-eucalyptus	Char	7.99	127.7	1.97
PR	Dry-pine	α-pine	8.944	119.564	5.50
	α-pine	β-pine	9.001	118.841	1.79
	β-pine	Char	7.999	110.162	3.50

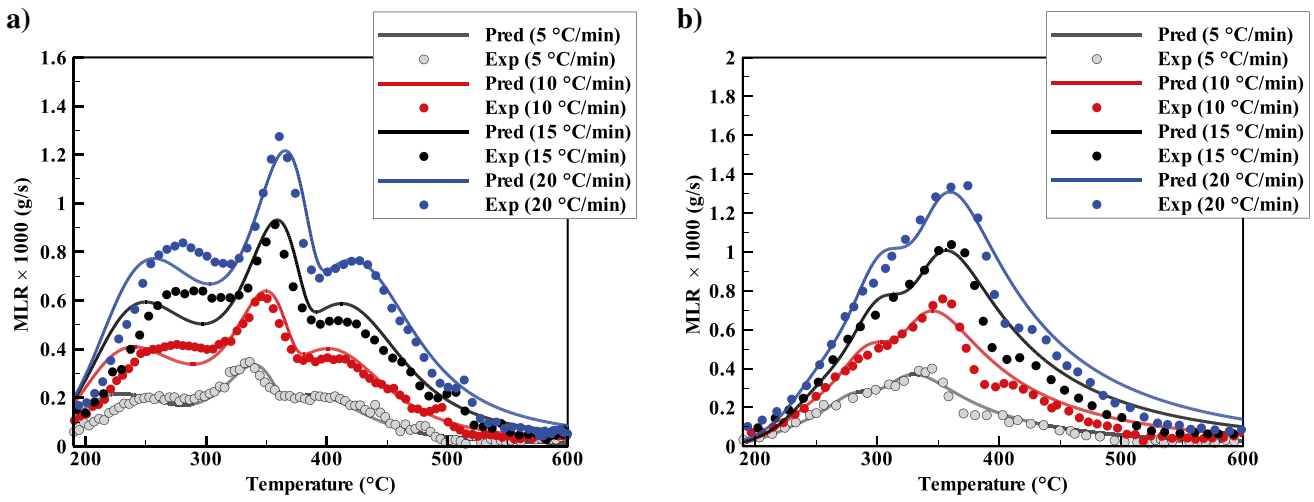

Fig. 3 Comparison of experimental and predicted MLR for **a** EG leaves and **b** PR needles under inert atmosphere (N2) for the four different heating rates

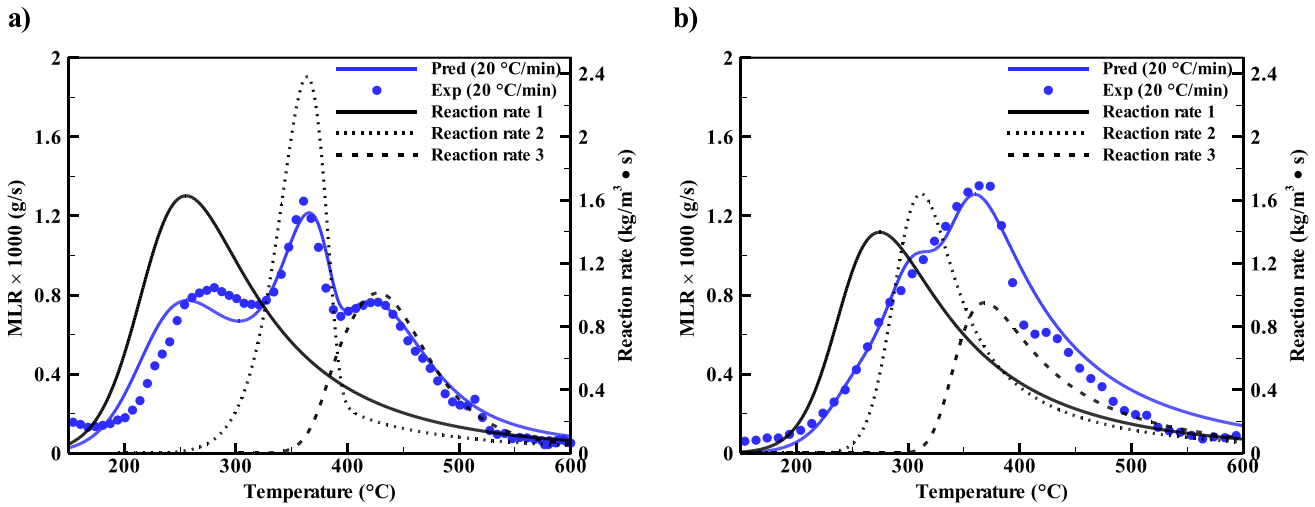

Fig. 4 Predicted reaction rates of **a** EG leaves and **b** PR needles under an inert atmosphere for a heating rate of 20 °C/min

to char, produces the second shoulder at around 420 °C. All reaction rates overlap at around 350 °C and attain similar decomposition rates at increasing temperatures. For PR needles (Fig. 4b), although the first reaction—the conversion of DWF into α-pine and gaseous pyrolysis products—begins around 200 °C, because it decays at 270 °C, it is not representative of the shoulder at 300 °C. Rather, the α-pine to β-pine conversion produces the shoulder at around the 300 °C. The third reaction, β-pine to char, begins around 300 °C (position of the shoulder), where a complete overlap of all three reactions begins. This third reaction sustains MLR until peak magnitude at around 370 °C.

3.3 Experimental results under oxidative atmosphere

To explore the oxidative reactivity of species and the effect of oxygen on thermal decomposition, the same TGA methodology as before was employed, though now under an oxidative atmosphere (air). Figure 5 shows the mass evolutions of EG leaves and PR needles under an oxidative atmosphere (air) as a function of the temperature for the four heating rates.

Both EG leaves (Fig. 5a) and PR needles (Fig. 5b) have similar ML curves at the four heating rates. For EG leaves, depending on the heating rate, 5–9% of the mass is lost between 200 and 250 °C; between 250 °C and 350 °C, 45% of the mass was lost; from 350 to 430 °C, 60% of the initial mass (comparable to the inert atmosphere, where char is the main species); and between 430 and 470 °C, 25% of the initial mass was devolatilized. At the end of the test, the residual mass is around 10% of the initial mass, regardless of the heating rate.

Figure 5b shows the mass evolution of PR needles under air as a function of temperature: between 200 and 250 °C, around 3% of the initial mass is devolatilized; from 250 to 350 °C—and a significant decrease for all heating rates—40 to 50% of the mass, for 20 and 5 °C min^{-1}, respectively; between 350 and 420 °C, 70% mass loss; and from 420 °C—i.e., the same temperature for complete

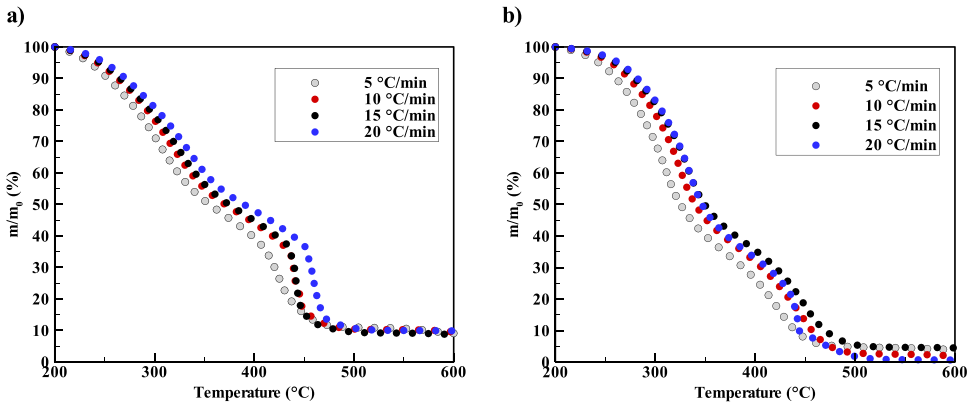

Fig. 5 Evolution of mass as a function of the temperature during the thermal decomposition under air for **a** EG leaves and **b** PR needles for the four heating rates

pyrolytic devolatilization—to 470 °C, the char oxidation process leaves only 3–5% of the initial mass as residue at the end of the test. The difference in mass remaining at the end of the test is likely due to the higher presence of ash content in EG leaves over PR needles (see Table 1). When mass loss under inert and oxidative atmosphere is compared (Figs. 1 and 5), there is a second decomposition thermal gradient peak between 430 and 470 °C, which can be attributed to the oxidation of lignin, pyrolysis, and char, and is clearly higher in the experiment under air conditions [70, 71].

Figure 6 presents the derived MLR curves as a function of temperature for the different heating rates under oxidative conditions. Similar to results under an inert atmosphere, the thermal decomposition process of EG leaves and PR needles occur in the same manner, independent of the heating rate value. However, the heating rate increases MLR intensity under air, confirming the literature on Eucalyptus leaves [72] and other solid materials like plywood [73]—and magnitude. Notably, the whole process occurs over two stages, with two peaks: the first, between 300 and 350 °C, and the second, between 400 and 450 °C. Under oxidative conditions, although peak temperature timing was independent of species, their magnitude was inverted between species. For EG leaves, the maximum peak occurs at around 450 °C, and for PR needles, at 330 °C. The oxidative process is thus more intense, with a lower duration, for EG leaves than for PR needles, explaining the additional mass at the end of the test.

For EG leaves (Fig. 6a), regardless of heating rate, MLR begins at around 200 °C; increases to a peak at 300 °C for 5 °C min^{-1}, and 340 °C, for 20 °C min^{-1}; decreases to around 420 °C—where the oxidative process begins (Fig. 5a); increases rapidly to the maximal peak at 420 and 450 °C, depending on heating rate; and finally ends at around 500 °C. Figure 6b shows a similar MLR in PR needles; however, the magnitudes of the two peaks are inverted, reaching maximum in the first peak at around 340 °C.

3.4 Estimations under oxidative atmosphere

The same evolutionary optimization method was implemented to obtain kinetics parameters for subsequent simulations to verify against experimental results. The optimization process includes the reaction order's local oxygen mass fraction. The optimized parameters obtained for EG leaves and PR needles with the SCE method are shown in Table 3.

To assess the six-step mechanism proposed in [74] under an oxidative atmosphere, the optimized parameters obtained via SCE were used as simulation inputs. The experimental and predicted MLR curves are presented in Fig. 7 for EG leaves (a) and PR needles (b). The simulated curve for EG leaves (Fig. 7a) correctly captures the peak magnitude and position for all heating rates between 250 and 350 °C; the decrease in MLR up to 380 °C; and, depending on heating rates, the second peak between 420 and 450 °C. For all heating rates except 5 °C min^{-1}, peak MLR magnitude was underpredicted. Interestingly, these results come from an undefined local oxygen mass fraction reaction order in the optimization process; though, outside the scope of the present work, future research should conduct sensitivity analyses for oxygen influence on the kinetics mechanism tested.

Figure 7b compares predicted six-step kinetics mechanisms and experimental MLR for PR needles. The entire oxidative pyrolysis behavior of these tests was captured. At higher heating rates, the occurrence of the first peak is predicted well—and to a lesser degree, the magnitude; and, at lower heating rates, 5 °C min^{-1}, the magnitude is well reproduced, but not the position. After the first peak, the model fits well with experimental MLR, predicting the valley, the second peak at around 450 °C, and the final decrease to the end of the test.

Each reaction of the complex mechanisms in simulated MLR at a heating rate of 20 °C min^{-1} is explored for EG leaves (Fig. 8a) and PR needles (Fig. 8b). For EG leaves, the R1 converting DWF to α-eucalyptus begins at around 200 °C and is responsible for the first shoulder, but not the peak at 340 °C; R2, converting α-eucalyptus to β-eucalyptus,

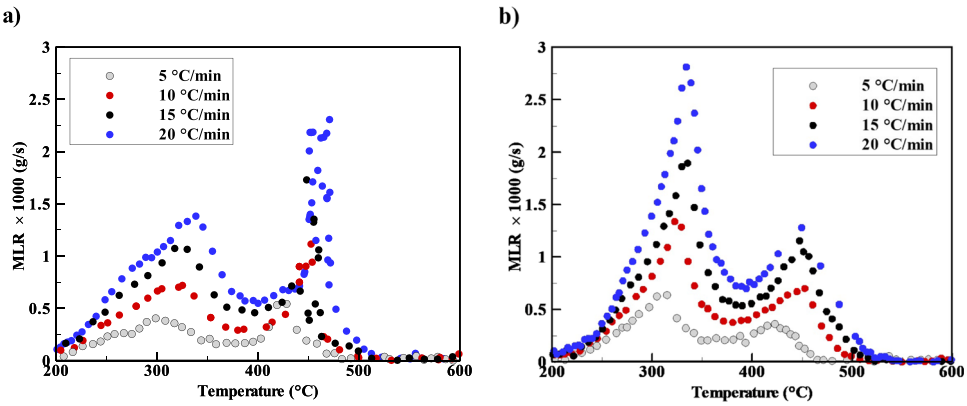

Fig. 6 Evolution of MLR as a function of the temperature during the thermal decomposition under air for **a** EG leaves and **b** PR needles for the four heating rates

Table 3 Estimated kinetics parameters under oxidative atmosphere for EG and PR

Species	Atm	Reagent	Product	Kinetics parameters			
				Log_A (s^{-1})	E_a (kJ mol^{-1})	n (-)	nO_2
EG	N_2	Dry-eucalyptus	α-eucalyptus	8.68	109.99	5.47	(-)
	N_2	α-eucalyptus	β-eucalyptus	9.14	126.52	1.00	(-)
	Air	α-eucalyptus	β-eucalyptus	6.00	119.60	0.16	0.80
	N_2	β-eucalyptus	Char	7.30	121.19	4.69	(-)
	Air	β-eucalyptus	Char	10.91	169.83	1.11	0.14
	Air	Char	Residue	11.03	132.64	3.05	0.47
PR	N_2	Dry-pine	α-pine	8.92	109.83	2.78	1.00
	N_2	α-pine	β-pine	8.85	149.87	1.45	(-)
	Air	α-pine	β-pine	6.59	90.66	0.58	1.18
	N_2	β-pine	Char	5.68	62.29	4.59	(-)
	Air	β-pine	Char	7.85	192.50	2.72	1.10
	Air	Char	Residue	10.51	164.63	0.86	1.24

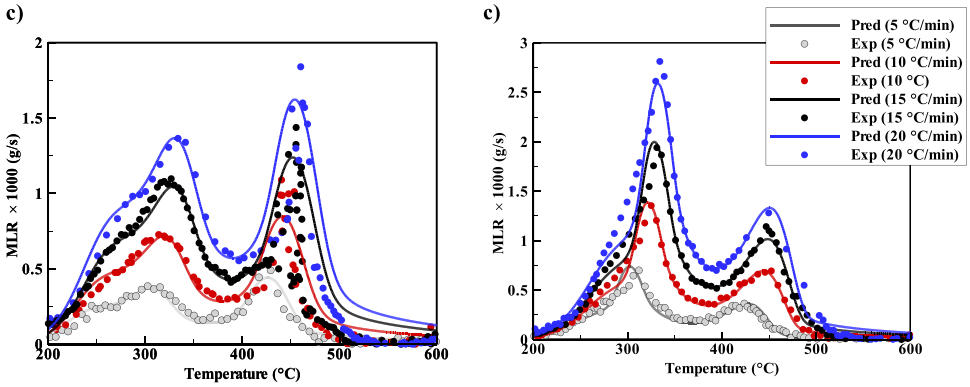

Fig. 7 Comparison of experimental and predicted MLR for **a** EG leaves and **b** PR needles under oxidative atmosphere (air) at four different heating rates

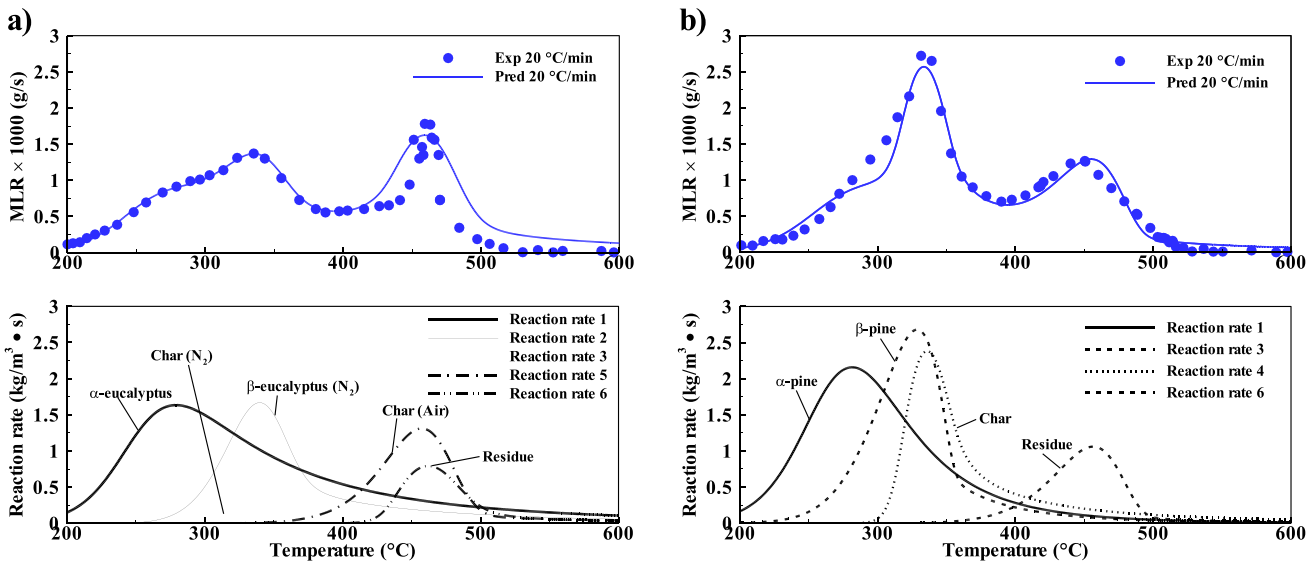

Fig. 8 Evolution of the predicted reaction rates for **a** EG leaves and **b** PR needles

begins around 250 °C; R3, α-eucalyptus to β-eucalyptus, is smaller than R2, but helps to attain maximum MLR; and R4 ($(\alpha - Specie) \rightarrow \nu_4(\beta - Specie) + (1 - \nu_4)Gas$) is interestingly negligible, reducing the initial mechanism from 6 to 5 reactions. This char (R5) and residue (R6) production are still responsible for the second peak at around 460 °C, with a complete overlap from 420 °C to the end of the test.

The PR needle model (Fig. 8b) thus had good agreement with just four reactions, and not the six proposed, since R3 and R5 were utterly negligible. Specifically, R1 goes from around 200 to 250 °C, producing α-pine from DWF; followed by the production of β-pine (R3) and char (R4), which begins around 300 °C. At this temperature, reactions R1, R3, and R4 overlap and produce the first and main peak around 330 °C. Notably, contributions from R2 (conversion of α-pine to β-pine under O_2) and R5 (conversion of β-pine to Char under air) are negligible. The char reaction (R6) oxidation nearly produces the second peak by itself at around 450 °C. A complete study on the effects of oxygen on reaction rates is recommended.

That means that in the presence of oxygen, the production of the intermediate species ($\beta -$ Specie) decreased at higher temperatures and is only formed by the ($\alpha -$ Specie) in R3. Effectively, this performance of the complex mechanism is part of the calculation result, as the one used in the present study was developed by the analysis of the gas emissions recorded with a FTIR spectrometer at the outlet of the TGA device [74]. Similar results were found in [75] for the study of treated plywood where two additional oxidative reactions were needed to describe the thermal decomposition of the material. It could be explained according to the organic composition of these wildland fuels, the shares of cellulose, hemicellulose, and lignin that may influence the phenomenon behavior. For the case of *Pinus radiata* (PR) needles, the mass of dry pine (DWF) decreases to form $\alpha -$ Pine (R1), which in turn will decompose to form $\beta -$ Pine (R2 and R4). Finally, wildland fuel is reduced after char and residue formation. Here, $\beta -$ Pine is formed by $\alpha -$ Pine under oxidative conditions (R4) one order of magnitude higher than in R2 under inert conditions. The reaction rates set found in this study for PR are qualitatively similar to those found in [20] for Mediterranean Pinus Pinaster.

4 Concluding remarks

The thermal decomposition kinetics behaviors of two Chilean wildland fuels, EG leaves and PR needles, were studied at different heating rates under two different inert and oxidative atmosphere conditions (N_2 and air) via TGA experiments. The SCE algorithm method was used to determine solid-phase thermal decomposition and oxidative kinetics parameters by correlating several reaction mechanisms under each atmosphere condition. A three-step mechanism for these two species for inert conditions with a set of 9 kinetic parameters for both was able to predict the thermal decomposition behavior. Results under oxidative atmospheres differed by species. The six-reaction oxidative mechanism proposed by Fateh et al. [74] was assessed for Mediterranean pine (*Pinus pinaster*) and tested previously by Benkorichi et al. [20] to simulate the thermal decomposition of species studied in the present work but found that a single-step mechanism can describe char oxidation, regardless of the species. The results of the present study show that the experimental TGA for thermal decomposition under oxidative conditions can be predicted with a good fit using five reactions for EG leaves and four reactions for PR needles. From the optimization process carried out with the SCE method, we consequently propose a set of 18 and 15 kinetics parameters for EG leaves and PR needles' thermal decomposition process, respectively. These results can be useful for minimizing computational resources in numerical simulations of pyrolysis or biomass oxidation. Further studies are necessary to extend the optimization of kinetic parameters for native and endemic species, in order to generate new forest strategies in the near future.

Supplementary Information The online version contains supplementary material available at https://doi.org/10.1007/s13399-022-03567-x.

Acknowledgements The authors would like to thank the support of the National Agency for Research and Development (ANID) Chile through the program Fondecyt/Iniciación 11161045 and ANID/Scholarship Program/DOCTORADO BECAS CHILE/2021 – 21211230.

Author contribution Andrés Arriagada: conceptualization; methodology; formal analysis; visualization; writing—review and editing; supervision. Jorge Contreras: conceptualization; methodology; formal analysis; visualization; writing—review and editing; supervision. Jean-Louis Consalvi: conceptualization; methodology; formal analysis; visualization; writing—review and editing; supervision.

Funding This research was funded by the National Agency for Research and Development (ANID) Chile through the program Fondecyt/Iniciación 11161045 and the ANID/Scholarship Program/DOCTORADO BECAS CHILE/2021 – 21211230.

Data availability The data presented in the study is available on request from the corresponding author.

Declarations

Ethical approval Not applicable.

Competing interests The authors declare no competing interests.

References

1. (CONAF) CNF (2020) Resumen nacional ocurrencia y daño por incendios forestales 1977–2020

2. Moore PF (2019) Global wildland fire management research needs. Current Forestry Reports 5:210–225. https://doi.org/10.1007/s40725-019-00099-y
3. Reszka P, Fuentes A (2015) The great Valparaiso fire and fire safety management in Chile. Fire Technol 51:753–758. https://doi.org/10.1007/s10694-014-0427-0
4. Guerrero, F., Hernández, C., Toledo, M., Espinoza, L., Carrasco, Y., Arriagada, A., Muñoz, A., Taborga, L., Bergmann, J., Carmona C (2021) Leaf thermal and chemical properties as natural drivers of plant flammability of native and exotic tree species of the Valpara í so Region , Chile. 1–24
5. Guerrero F, Carmona C, Hernández C, et al (2022) Drivers of flammability of Eucalyptus globulus Labill leaves: terpenes, essential oils, and moisture content. Forests 13:. https://doi.org/10.3390/f13060908
6. Coropración Nacional Forestal (2013) CONAF, por un Chile forestal sustentable. http://www.conaf.cl/wp-content/files_mf/1382992046CONAFporunChileForestalSustentable.pdf. Accessed 3 Oct 2022
7. Shahbaz M, Yusup S, Inayat A et al (2017) Optimization of hydrogen and syngas production from PKS gasification by using coal bottom ash. Bioresour Technol 241:284–295. https://doi.org/10.1016/j.biortech.2017.05.119
8. Zhang B, Zhang L, Yang Z, He Z (2017) An experiment study of biomass steam gasification over NiO/dolomite for hydrogen-rich gas production. Int J Hydrogen Energy 42:76–85. https://doi.org/10.1016/j.ijhydene.2016.10.044
9. Reszka P, Cruz JJ, Valdivia J et al (2020) Ignition delay times of live and dead pinus radiata needles. Fire Saf J 112:102948. https://doi.org/10.1016/j.firesaf.2020.102948
10. Rothermel RC (1972) A mathematical model for predicting fire spread in wildland fuels. Res. Pap. INT-115. Ogden, UT: U.S. Department of Agriculture, Intermountain Forest and Range Experiment Station. 40 p
11. Debiagi PEA, Gentile G, Pelucchi M et al (2016) Detailed kinetic mechanism of gas-phase reactions of volatiles released from biomass pyrolysis. Biomass Bioenergy 93:60–71. https://doi.org/10.1016/j.biombioe.2016.06.015
12. Debiagi PEA, Pecchi C, Gentile G et al (2015) Extractives extend the applicability of multistep kinetic scheme of biomass pyrolysis. Energy Fuels 29:6544–6555
13. Safi MJ, Mishra IM, Prasad B (2004) Global degradation kinetics of pine needles in air. Thermochim Acta 412:155–162. https://doi.org/10.1016/j.tca.2003.09.017
14. Jolly WM, Parsons RA, Hadlow AM et al (2012) Relationships between moisture, chemistry, and ignition of Pinus contorta needles during the early stages of mountain pine beetle attack. For Ecol Manage 269:52–59. https://doi.org/10.1016/J.FORECO.2011.12.022
15. Larini M, Giroud F, Porterie B, Loraud J-C (1998) A multiphase formulation for fire propagation in heterogeneous combustible media. Int J Heat Mass Transf 41:881–897. https://doi.org/10.1016/S0017-9310(97)00173-7
16. Porterie B, Consalvi J-L, Loraud J-C et al (2007) Dynamics of wildland fires and their impact on structures. Combust Flame 149:314–328. https://doi.org/10.1016/j.combustflame.2006.12.017
17. Morvan D, Dupuy JL (2001) Modeling of fire spread through a forest fuel bed using a multiphase formulation. Combust Flame 127:1981–1994. https://doi.org/10.1016/S0010-2180(01)00302-9
18. Morvan D, Méradji S, Accary G (2009) Physical modelling of fire spread in Grasslands. Fire Saf J 44:50–61. https://doi.org/10.1016/J.FIRESAF.2008.03.004
19. Morvan D (2015) Numerical study of the behaviour of a surface fire propagating through a firebreak built in a Mediterranean shrub layer. Fire Saf J 71:34–48. https://doi.org/10.1016/J.FIRESAF.2014.11.012
20. Benkorichi S, Fateh T, Richard F et al (2017) Investigation of thermal degradation of pine needles using multi-step reaction mechanisms. Fire Saf J 91:811–819. https://doi.org/10.1016/j.firesaf.2017.03.058
21. López-González D, Fernandez-Lopez M, Valverde JL, Sanchez-Silva L (2013) Thermogravimetric-mass spectrometric analysis on combustion of lignocellulosic biomass. Bioresour Technol 143:562–574. https://doi.org/10.1016/J.BIORTECH.2013.06.052
22. Chen R, Li Q, Zhang Y et al (2019) Pyrolysis kinetics and mechanism of typical industrial non-tyre rubber wastes by peak-differentiating analysis and multi kinetics methods. Fuel 235:1224–1237. https://doi.org/10.1016/J.FUEL.2018.08.121
23. Jiang L, Zhang D, Li M et al (2018) Pyrolytic behavior of waste extruded polystyrene and rigid polyurethane by multi kinetics methods and Py-GC/MS. Fuel 222:11–20. https://doi.org/10.1016/J.FUEL.2018.02.143
24. Anca-Couce A (2016) Reaction mechanisms and multi-scale modelling of lignocellulosic biomass pyrolysis. Prog Energy Combust Sci 53:41–79. https://doi.org/10.1016/j.pecs.2015.10.002
25. Anca-Couce A, Scharler R (2017) Modelling heat of reaction in biomass pyrolysis with detailed reaction schemes. Fuel 206:572–579. https://doi.org/10.1016/j.fuel.2017.06.011
26. Dimitrakopoulos AP (2001) Thermogravimetric analysis of Mediterranean plant species. J Anal Appl Pyrolysis 60:123–130. https://doi.org/10.1016/S0165-2370(00)00164-9
27. Tihay V, Gillard P (2010) Pyrolysis gases released during the thermal decomposition of three Mediterranean species. J Anal Appl Pyrolysis 88:168–174. https://doi.org/10.1016/j.jaap.2010.04.002
28. Gerandi G, Tihay-Felicelli V, Santoni P-A et al (2019) Multi-scale modeling of the degradation of thermally thin wood plates. Fire Saf J 108:102823. https://doi.org/10.1016/j.firesaf.2019.102823
29. Burra KRG, Gupta AK (2019) Modeling of biomass pyrolysis kinetics using sequential multi-step reaction model. Fuel 237:1057–1067. https://doi.org/10.1016/j.fuel.2018.09.097
30. Amini E, Safdari M-S, Weise DR, Fletcher TH (2019) Pyrolysis kinetics of live and dead wildland vegetation from the Southern United States. J Anal Appl Pyrolysis 142:104613. https://doi.org/10.1016/J.JAAP.2019.05.002
31. Cumming JW, McLaughlin J (1982) The thermogravimetric behaviour of coal. Thermochim Acta 57:253–272. https://doi.org/10.1016/0040-6031(82)80037-3
32. Cai J, Wang Y, Zhou L, Huang Q (2008) Thermogravimetric analysis and kinetics of coal/plastic blends during co-pyrolysis in nitrogen atmosphere. Fuel Process Technol 89:21–27. https://doi.org/10.1016/J.FUPROC.2007.06.006
33. Àgueda A, Liodakis S, Pastor E, Planas E (2009) Characterization of the thermal degradation and heat of combustion of Pinus halepensis needles treated with ammonium-polyphosphate-based retardants. J Therm Anal Calorim 98:235–243. https://doi.org/10.1007/s10973-009-0134-0
34. Wadhwani R, Sutherland D, Moinuddin KAM, Joseph P (2017) Kinetics of pyrolysis of litter materials from pine and eucalyptus forests. J Therm Anal Calorim 130:2035–2046. https://doi.org/10.1007/s10973-017-6512-0
35. Richter F, Rein G (2020) Reduced chemical kinetics for micro-scale pyrolysis of softwood and hardwood. Bioresour Technol 301:122619. https://doi.org/10.1016/j.biortech.2019.122619
36. McGrattan K, Klein B, Hostikka S, Floyd J (2010) Fire dynamics simulator (version 5), user's guide. NIST Spec Publ 1019:1–186
37. Lautenberger C, Fernandez-Pello C (2009) A model for the oxidative pyrolysis of wood. Combust Flame 156:1503–1513. https://doi.org/10.1016/j.combustflame.2009.04.001
38. Stoliarov S, Lyon R (2008) Thermo-kinetic model of burning for pyrolyzing materials. Fire Safety Science 9:1141–1152

39. Ding Y, Wang C, Lu S (2015) Modeling the pyrolysis of wet wood using FireFOAM. Energy Convers Manag 98:500–506. https://doi.org/10.1016/j.enconman.2015.03.106
40. Ding Y, Ezekoye OA, Zhang J et al (2018) The effect of chemical reaction kinetic parameters on the bench-scale pyrolysis of lignocellulosic biomass. Fuel 232:147–153. https://doi.org/10.1016/j.fuel.2018.05.140
41. Ding Y, Fukumoto K, Ezekoye OA et al (2020) Experimental and numerical simulation of multi-component combustion of typical charring material. Combust Flame 211:417–429. https://doi.org/10.1016/j.combustflame.2019.10.016
42. Lautenberger C, Fernandez-Pello C (2009) Generalized pyrolysis model for combustible solids. Fire Saf J 44:819–839. https://doi.org/10.1016/j.firesaf.2009.03.011
43. Ahmaruzzaman M (2008) Proximate analyses and predicting HHV of chars obtained from cocracking of petroleum vacuum residue with coal, plastics and biomass. Bioresour Technol 99:5043–5050. https://doi.org/10.1016/j.biortech.2007.09.021
44. Lautenberger C, Rein G, Fernandez-Pello C (2006) The application of a genetic algorithm to estimate material properties for fire modeling from bench-scale fire test data. Fire Saf J 41:204–214. https://doi.org/10.1016/J.FIRESAF.2005.12.004
45. Ding Y, Wang C, Chaos M et al (2016) Estimation of beech pyrolysis kinetic parameters by shuffled complex evolution. Bioresour Technol 200:658–665. https://doi.org/10.1016/J.BIORTECH.2015.10.082
46. Duan QY, Gupta VK, Sorooshian AS, Dixon LCW (1993) Shuffled complex evolution approach for effective and efficient global minimization. J Optim Theory Appl 76:501–521. https://doi.org/10.1007/BF00939380
47. Hasalová L, Ira J, Jahoda M (2016) Practical observations on the use of shuffled complex evolution (SCE) algorithm for kinetic parameters estimation in pyrolysis modeling. Fire Saf J 80:71–82. https://doi.org/10.1016/j.firesaf.2016.01.007
48. Leroy V, Cancellieri D, Leoni E, Rossi J-L (2010) Kinetic study of forest fuels by TGA: model-free kinetic approach for the prediction of phenomena. Thermochim Acta 497:1–6. https://doi.org/10.1016/j.tca.2009.08.001
49. Lautenberger C, Fernandez-Pello AC (2011) Optimization algorithms for material pyrolysis property estimation. Fire Safety Science 10:751–764
50. Purnomo DMJ, Richter F, Bonner M et al (2020) Role of optimisation method on kinetic inverse modelling of biomass pyrolysis at the microscale. Fuel 262:116251. https://doi.org/10.1016/J.FUEL.2019.116251
51. Yuen ACY, Chen TBY, Wang C et al (2020) Utilising genetic algorithm to optimise pyrolysis kinetics for fire modelling and characterisation of chitosan/graphene oxide polyurethane composites. Compos B Eng 182:107619. https://doi.org/10.1016/J.COMPOSITESB.2019.107619
52. Park T-Y, Froment GF (1998) A hybrid genetic algorithm for the estimation of parameters in detailed kinetic models. Comput Chem Eng 22:S103–S110. https://doi.org/10.1016/S0098-1354(98)00043-X
53. Chang Y, Jia M, Niu B et al (2018) Construction of a skeletal oxidation mechanism of n-pentanol by integrating decoupling methodology, genetic algorithm, and uncertainty quantification. Combust Flame 194:15–27. https://doi.org/10.1016/J.COMBUSTFLAME.2018.04.012
54. Elliott L, Ingham DB, Kyne AG et al (2004) Genetic algorithms for optimisation of chemical kinetics reaction mechanisms. Prog Energy Combust Sci 30:297–328. https://doi.org/10.1016/J.PECS.2004.02.002
55. Fiola G (2019) Fiola G (2019) Improving inverse analysis of pyrolysis model parametrization using hill climbing algorithms. University of Maryland. https://doi.org/10.13016/73q9-6f3r
56. Lautenberger C (2007) A Generalized Pyrolysis Model for Combustible Solids. UC Berkeley: Combustion Processes Laboratories. Retrieved from https://escholarship.org/uc/item/7wz5m7dg
57. Leoni E, Tomi P, Khoumeri B et al (2001) Thermal degradation of Pinus pinaster needles by DSC. Part 1: Dehydration kinetics. J Fire Sci 19:379–397. https://doi.org/10.1106/QBDC-5VH2-U5X2-FUF7
58. Leoni E, Cancellieri D, Balbi N, Tomi, P, Bernardini AF, Kaloustian J, Marcelli T (2003) Thermal Degradation of Pinus Pinaster Needles by DSC, Part 2: Kinetics of Exothermic Phenomena. J Fire Sci 21:117–130. https://doi.org/10.1177/0734904103021002002
59. Severino G, Cabrera A, Contreras J, et al (2020) A new burner to characterize laminar diffusion flames generated from wildland fuels. Fire Saf J 102947. https://doi.org/10.1016/J.FIRESAF.2020.102947
60. Damartzis T, Vamvuka D, Sfakiotakis S, Zabaniotou A (2011) Thermal degradation studies and kinetic modeling of cardoon (Cynara cardunculus) pyrolysis using thermogravimetric analysis (TGA). Bioresour Technol 102:6230–6238. https://doi.org/10.1016/j.biortech.2011.02.060
61. McKendry P (2002) Energy production from biomass (part 2): conversion technologies. Bioresour Technol 83:47–54. https://doi.org/10.1016/S0960-8524(01)00119-5
62. Parikh J, Channiwala SA, Ghosal GK (2007) A correlation for calculating elemental composition from proximate analysis of biomass materials. Fuel 86:1710–1719. https://doi.org/10.1016/j.fuel.2006.12.029
63. Gominho J, Lourenço A, Miranda I, Pereira H (2012) Chemical and fuel properties of stumps biomass from Eucalyptus globulus plantations. Ind Crops Prod 39:12–16. https://doi.org/10.1016/j.indcrop.2012.01.026
64. Shen J, Zhu S, Liu X et al (2010) The prediction of elemental composition of biomass based on proximate analysis. Energy Convers Manag 51:983–987. https://doi.org/10.1016/j.enconman.2009.11.039
65. Cuiping L, Chuangzhi W, Yanyongjie HH (2004) Chemical elemental characteristics of biomass fuels in China. Biomass Bioenergy 27:119–130. https://doi.org/10.1016/j.biombioe.2004.01.002
66. Chen Z, Zhu Q, Wang X et al (2015) Pyrolysis behaviors and kinetic studies on Eucalyptus residues using thermogravimetric analysis. Energy Convers Manag 105:251–259. https://doi.org/10.1016/j.enconman.2015.07.077
67. Costa VJ, Vieira RM, Girotto SBFT, Simioni FJ (2016) Pyrolysis and thermogravimetry of blended and nonblended residues of pine and eucalyptus forestry woods. Environ Prog Sustain Energy 35:1521–1528. https://doi.org/10.1002/ep.12372
68. Di Blasi C (2008) Modeling chemical and physical processes of wood and biomass pyrolysis. Prog Energy Combust Sci 34:47–90. https://doi.org/10.1016/j.pecs.2006.12.001
69. Shafizadeh F (1985) Pyrolytic reactions and products of biomass. In: Fundamentals of thermochemical biomass conversion. Springer, pp 183–217
70. Liu N, Wang B, Fan W (2003) Kinetic compensation effect in the thermal decomposition of biomass in air atmosphere. Fire Safety Science 7:581–592. https://doi.org/10.3801/IAFSS.FSS.7-581
71. Font R, Marcilla A, Verdti E, Devesa J (1991) Thermogravimetric kinetic study of the pyrolysis of almond shells and almond shells impregnated with CoCl. J Analytical Appl Pyrolysis 21(3):249–264. https://doi.org/10.1016/0165-2370(91)80001-O
72. Zanuncio AJV, Motta JP, da Silveira TA et al (2013) Physical and colorimetric changes in Eucalyptus grandis wood after heat treatment. BioResources 9:293–302
73. Fateh T, Richard F, Batiot B et al (2016) Characterization of the burning behavior and gaseous emissions of pine needles in a cone

calorimeter – FTIR apparatus. Fire Saf J 82:91–100. https://doi.org/10.1016/J.FIRESAF.2016.03.008
74. Fateh T, Richard F, Zaida J et al (2016) Multi-scale experimental investigations of the thermal degradation of pine needles. Fire Mater 41:654–674. https://doi.org/10.1002/fam.2407
75. Fateh T, Rogaume T, Luche J et al (2013) Modeling of the thermal decomposition of a treated plywood from thermo-gravimetry and Fourier-transformed infrared spectroscopy experimental analysis. J Anal Appl Pyrolysis 101:35–44. https://doi.org/10.1016/J.JAAP.2013.02.015